12

Electronic structure of variants of compositions of scandate and nickel-oxide cathodes of microwave devices

© V.I. Kapustin,[1] I.P. Li,[2] A.S. Serpichev,[1] A.V. Shumanov,[2] N.E. Kozhevnikova[2]

[1] MIREA - Russian Technological University,
119454 Moscow, Russia
[2] Pluton JSC,
105120 Moscow, Russia
e-mail: kapustin@mirea.ru

Received July 9, 2021
Revised November 28, 2021
Accepted December 8, 2021

By methods of electron spectroscopy for chemical analysis and spectroscopy of characteristic losses of electron energy, the electronic structure of barium oxide crystallites doped with other chemical elements, including scandium from scandium-containing phases, was investigated. The physical and physicochemical conditions are formulated, the fulfillment of which allows to form the electronic structure of the scandate cathode with a high level of thermionic emission: the achievement of the minimum ratio of the surface volume concentration of oxygen vacancies and the maximum distance between the top of the valence band and the Fermi level.

Keywords: microwave devices, cathodes, thermionic emission, output operation, electronic structure, electron spectroscopy.

DOI: 10.21883/TP.2022.03.53270.211-21

Introduction

Since the 1990s, scientific laboratories of the universities and industrial enterprises in all developed countries perform the studies aimed at creation of so called scandate cathodes, i.e. scandium-containing matrix-type cathodes. Based on the results of studies it was established, that such a cathode could provide for reaching the thermionic emission current density of up to 100 A/cm^2, and, perspectively, up to 400 A/cm^2 [1–6]. It enables creation of fundamentally innovative types of the electrical vacuum microwave devices. At the same time, the obtained results refer to a poor technological reproducibility of the emission properties of scandate cathodes, therefore, until now, neither industrial enterprise has successfully deployed serial manufacture of microwave devices with the cathodes of that type.

Figure 1 shows the diagram of potential ways of creation of cathode material with the specified emission properties. In accordance with this diagram, scientific methodology of the major of publications could be classified as the study of the area (interface) 1 thereof, when various process techniques are adopted for manufacture of the cathode and a series of emission properties of the technology product are measured, such as thermal emission and secondary emission properties, stability and durability of the properties, permissible temperature interval of operation of the cathode material.

Since the emission properties of the cathode material are determined by the electron structure of the active emission phase of the material (BaO crystallites), the process of such phase formation at the cathode activation stage is determined by the original phase composition of the material, original microstructure of the material, micro admixtures impregnating the active-phase composition from other phases at the cathode activation and operation stage. This is why „design“ of emission properties of cathode with the specified emission properties, in our opinion, is expedient to perform based on the results of the studies in the areas 2−5 in Fig. 1. When establishing the regularities in the areas 2−5 selection of technologies 6−8 that ensure formation of the required original phase composition and microstructure of the material, micro alloying of the active emission phase with necessary micro admixtures, will be

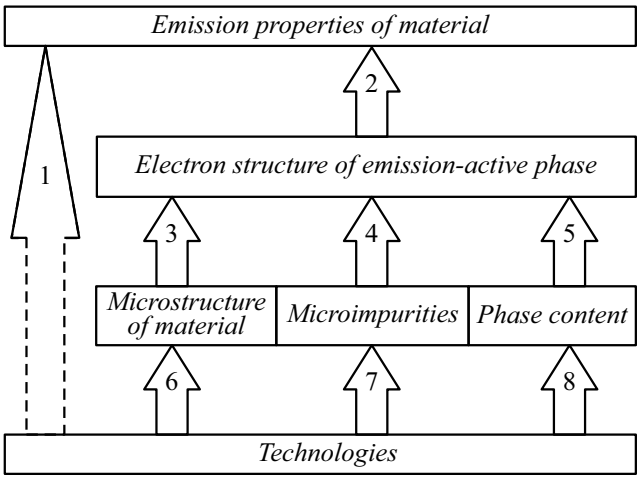

Figure 1. Diagram of development of the cathode material with specified emission properties.

predefined almost automatically based on the known set of possible process operations.

Expediency of the approach to creation of the cathode materials based on the study of the areas 2, 3 and 5 was put for the first time in the publications [7,8], and the importance of studying the area 4 was theoretically and experimentally ascertained in the studies [9–13], and the study [10] for the first time experimentally ascertained synergetic effect of impact of micro admixtures of calcium and strontium to the electron structure of barium oxide crystallites. The obtained experimental and theoretical results for the various types of cathode materials were generalized in the monograph [14].

Along with that possible joint (synergetic) manifestation of impact of micro admixtures in BaO crystallites to its electron structure appeared to be insufficiently studied, as well as the impact of phase state, in particular, of scandium-containing components, to the electron structure of active emission phase of the cathode material and synergetics of its micro alloying with micro admixtures. This is why the purpose of this work was the study of electron structure of materials and search for effects, including synergetic ones, the impact of micro admixtures in BaO on two parameters that determine the value of its work function: achievement of the minimum ratio of the surface and volume concentration of oxygen vacancies and the maximum distance between the top of valence band and the Fermi level.

1. Experimental samples and methodologies of studies

Two groups of experimental samples were manufactured for the study of impact of micro alloying to the electron structure of BaO crystallites, first of all, to the volume and surface concentration of oxygen vacancies in BaO crystallites, as well as for the study of potential synergetic effect of double alloying.

The first group includes sample materials in the form of a disc with the diameter of 7 mm and the thickness of 1 mm produced by baking and further pressing of discs made of mixture of barium carbonate powder and powders of additional components in the number of 10% (by weight) — oxides of yttrium, rhenium, palladium, and strontium carbonate. The powders were baked in vacuum at the temperature of 1200°C during 2 h on a nickel plate. Since nickel has a considerable volatility at this temperature, as a result of baking, BaO crystallites were formed in the material samples, containing oxygen vacancies, BaO crystallites containing oxygen vacancies and alloyed with the atoms of an additional component (yttrium, rhenium, palladium, strontium), as well as BaO crystallites containing oxygen vacancies and alloyed with atoms of an additional component and atoms of nickel.

The second group includes the samples of materials in the form of a disc with the diameter of 7 mm and the thickness of 1 mm, produced by baking and further pressing of mixture of tungsten powder (90% by weight), barium-calcium aluminate previously synthesized and ground in a powder of the composition $2.5BaO \cdot 0.4CaO \cdot Al_2O_3$ and additional components in the form of intermetallic compound powder Re_2Sc, powder of the $80\%W + 20\%Re$ alloy, and scandium hydride powder ScH_2. The powders were also baked in vacuum at the temperature of 1200°C during 2 h but on a tungsten plate. As a result of baking, BaO crystallites were formed in the material samples, containing oxygen vacancies, as well as BaO crystallites containing oxygen vacancies and, depending on the composition of mixtures, alloyed with atoms of tungsten, rhenium, scandium and combination of the specified elements.

Intermetallic compound powder Re_2Sc was produced by electric arc remelting of components in the medium of purified argon with further grinding in a ball mill. The powder of scandium hydride ScH_2 was produced by scandium annealing in the medium of hydrogen with further grinding in a ball mill. The powder of the alloy $80\%W + 20\%Re$ was produced at the Scientific and Production Complex „Advanced Powder Technologies“ (city of Tomsk) by diffusion of the wire VR-20 (alloy $80\%W + 20\%Re$) by the electric explosion method. The powder of the alloy VR-20 consists of particles with the diameter $1-2\,\mu$m and submicron grain-size particles of the powder.

Electron states of the elements in the materials samples were studied by using electron spectroscopy for chemical analysis (ESCA), and the spectra were interpreted by breakdown of peaks in ESCA spectra into Gauss peaks subject to impact of the atom surrounding by other elements to the atom peak shifts, which depend on the value of electronegativeness of the specified elements. As an example, Fig. 2 shows the structure of $3d_{5/2}$ electron level of barium in the sample of material $90\%BaCO_3 + 10\%Y_2O_3$, and Fig. 3 — structure of $3d_{5/2}$ and $3d_{3/2}$ electron level of yttrium in the same sample of material. Interpretation of electron states of barium and yttrium in the specified sample is given in Table 1 (cc. 1.1–1.4 correspond to *1–4* in Fig. 2) and in Table 2 (cc. 1–4 correspond to peaks *1–4* in Fig. 3).

The concentration of oxygen vacancies in the samples of materials was studied by the method of spectroscopy of characteristic losses of the energy of electrons (SCLEE) at the energy of initial electrons 1005 eV with the registration pitch 0.05 eV. In order to improve sensitivity of the method they performed digital differentiation of the spectra. As an example, Fig. 4 shows differential spectrum of characteristic losses of the energy of electrons in the sample of material $90\%BaCO_3 + 10\%Y_2O_3$. Characteristic losses of energy of electrons in the studied samples of materials are caused by excitation of surface and volume plasmons in metallic phase of materials from the second group of samples (tungsten), as well as by excitation of the surface and volume plasmons in barium oxide crystallites containing oxygen vacancies, which form donor-type point defects [7,8], and admixture atoms.

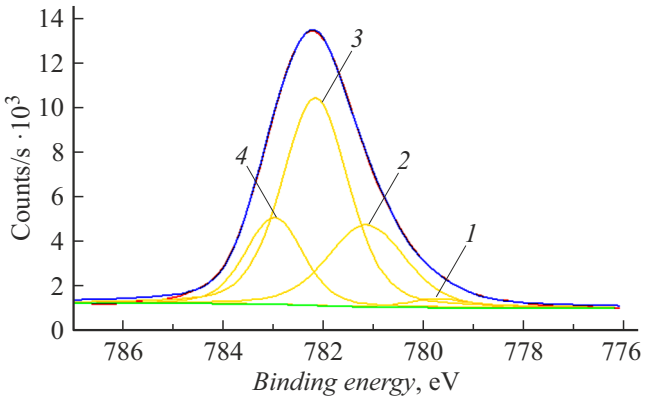

Figure 2. The structure of $3d_{5/2}$ electron level of barium in the sample of material $BaCO_3 + 10\%Y_2O_3$ annealed in vacuum at 1200°C during 2 h.

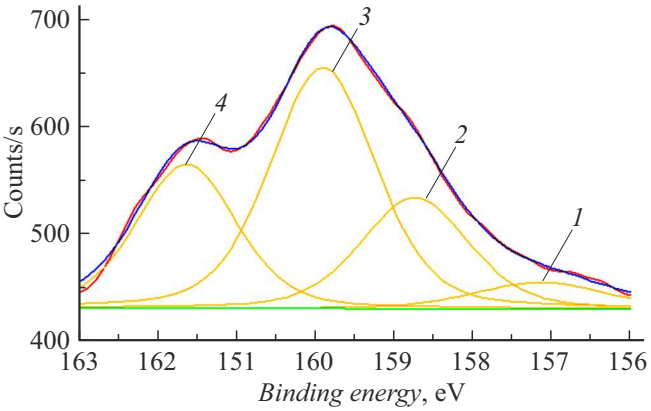

Figure 3. The structures of $3d_{5/2}$ and $3d_{3/2}$ electron levels of yttrium in the sample of material $BaCO_3 + 10\%Y_2O_3$ annealed in vacuum at 1200°C during 2 h.

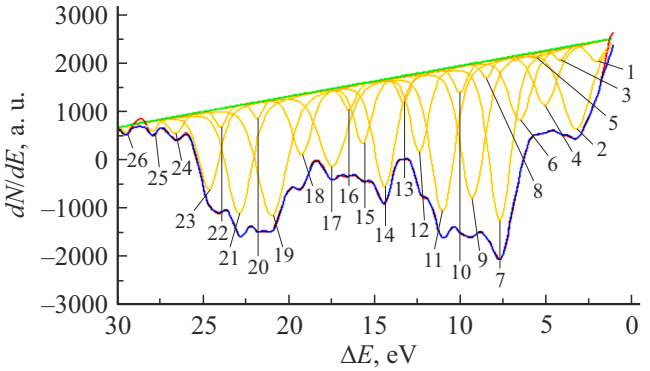

Figure 4. Spectrum of characteristic losses of energy of electrons in the sample of material $BaCO_3 + 10\%Y_2O_3$ annealed in vacuum at 1200°C during 2 h.

In this case the energies of excited surface ΔE_S and volume ΔE_D plasmons are related with the surface N_S and volume N_D concentration of oxygen vacancies by the ratios [14]:

$$\Delta E_D = \sqrt{\frac{e^{*2}\hbar^2 N_D}{\varepsilon\varepsilon_0 m^*}}, \quad \Delta E_S = \sqrt{\frac{e^{*2}\hbar^2 N_S}{2\varepsilon\varepsilon_0 m^*}}, \qquad (1)$$

where e^* — efficient charge of oxygen vacancy, m^* — efficient mass of electrons of oxygen vacancies, $\hbar$ — Planck's constant, ε_0 — dielectric constant, $\varepsilon = 3.6$ — high-frequency dielectric permeability of barium oxide. Then, the energy of plasma losses of electrons will be

$$\Delta E = n_1 \Delta E_D + n_2 \Delta E_S, \qquad (2)$$

where n_1 and n_2 are integer numbers.

For calculation of the surface and volume concentration of oxygen vacancies the values of efficient mass of electrons on oxygen vacancies and efficient charge of vacancies in pure BaO crystallites alloyed by the same type of micro admixtures were taken from [12] and [14], where these were determined experimentally by the optical absorption method. The values of specified parameters for BaO crystallites alloyed by two types of micro admixtures are not experimentally determined now. This is why for the case of double alloying when calculating by the ratios (1) and (2) they took the values of efficient mass and efficient charge for the component contained in the material with the maximum concentration. Such a selection could result in certain error in calculation of absolute values of the surface and volume concentrations of vacancies, but did not impact to a very important parameter — ratio of the surface and volume concentrations of vacancies in each sample.

When calculating the surface and volume concentrations of electrons in the metallic phase of samples of materials, formally, one may use the ratios (1) and (2), if for the metals $e^* = e$, $m^* = m$, $\varepsilon = 1$. As an example, Tables 3 and 4 include the diagram of interpretation of the spectrum of characteristic losses of the material sample with the composition $90\%BaCO_3 + 10\%Y_2O_3$.

Position of the edge of the valence band N_{VS} relative to the Fermi level E_F for the first group of materials was determined by the ESCA method, subject to the density of electron states near to the edge of the valence band $N_V(E)$ is described by approximate ratio

$$N_V(E) \approx \sqrt{|E_{VS} - E|}. \qquad (3)$$

In this case the dependence of the ESCA signal intensity square on the bond energy will be the straight line, whose extrapolation to the energy axis enables to determine the parameter E_{VS} relative to the Fermi level, as an example it shown in Fig. 5 for the sample of material with the composition $90\%BaCO_3 + 10\%Y_2O_3$. The values of the parameter E_{VS}, in turn, allow to determine both the value and direction of curvature of energetic bands V in barium oxide crystallites near to the surface [14]. Determination of the parameter E_{VS} for the second group of the materials was impossible, because in these samples the valence band of barium oxide crystallites is overlapped by the tungsten conductivity band.

Table 1. Interpretation of $3d_{5/2}$ electron spectra of barium in the samples of materials

№. of peak	Energy of peak, eV	Intensity of peak, counts/s	Width of peak, eV	Barium in the phase
1	$90\%BaCO_3 + 10\%Y_2O_3$			
1.1	779.70	404.39	1.40	$Ba(OH)_2 \cdot H_2O$
1.2	781.15	3670.98	1.83	$Ba_{(1-y-z)}O_{(1-x)}Ni_yY_z$
1.3	782.17	9302.08	1.57	$BaO_{(1-x)}$
1.4	782.99	3893.82	1.34	$Ba_{(1-y)}O_{(1-x)}Y_y$
2	$90\%BaCO_3 + 10\%Re$			
2.1	780.32	1845.19	1.80	$Ba_{(1-y-z)}O_{(1-x)}Ni_yRe_z$
2.2	781.71	13073.08	1.87	$BaO_{(1-x)}$
2.3	782.58	609.98	0.96	$Ba_{(1-y)}O_{(1-x)}Re_y$
3	$90\%BaCO_3 + 10\%Pd$			
3.1	780.64	2219.60	1.80	$Ba_{(1-y-z)}O_{(1-x)}Ni_yPd_z$
3.2	781.79	12472.40	1.88	$BaO_{(1-x)}$
3.3	782.61	1622.85	1.16	$Ba_{(1-y)}O_{(1-x)}Pd_y$
4	$90\%BaCO_3 + 10\%SrCO_3$			
4.1	780.55	1426.20	1.99	$Ba_{(1-y-z)}O_{(1-x)}Ni_ySr_z$
4.2	782.14	7593.82	1.85	$BaO_{(1-x)}$
4.3	783.07	1129.03	1.04	$Ba_{(1-y)}O_{(1-x)}Sr_y$
5	$90\%W + 5\%2.5BaO \cdot 0.4CaO \cdot Al_2O_3 + 5\%Re_2Sc$			
5.1	779.86	478.98	1.08	$Ba_{(1-y)}O_{(1-x)}W_y$
5.2	780.84	2176.37	1.98	Barium in barium-calcium aluminate
5.3	782.30	1174.76	1.55	$Ba_{(1-y)}O_{(1-x)}Sc_y$
5.4	782.66	192.66	0.72	$Ba_{(1-y)}O_{(1-x)}Al_y$
5.5	783.63	2364.52	1.96	$Ba_{(1-y-z)}O_{(1-x)}Re_ySc_z$
5.6	784.68	685.53	1.23	$Ba_{(1-y)}O_{(1-x)}Ca_y$
5.7	785.84	497.79	1.98	BaO_2
6	$90\%W + 5\%2.5BaO \cdot 0.4CaO \cdot Al_2O_3 + 5\%(80\%W + 20\%Re)$			
6.1	780.61	1978.24	1.74	Barium in barium-calcium aluminate
6.2	781.75	591.98	1.12	$BaO_{(1-x)}$
6.3	782.77	1656.22	1.66	$Ba_{(1-y)}O_{(1-x)}Re_y$
6.4	784.19	2550.55	1.99	$Ba_{(1-y-z)}O_{(1-x)}Re_yW_z$
6.5	785.66	860.26	1.99	BaO_2
7	$90\%W + 5\%2.5BaO \cdot 0.4CaO \cdot Al_2O_3 + 5\%ScH_2$			
7.1	780.26	1289.40	1.45	Barium in barium-calcium aluminate
7.2	781.36	2379.82	1.98	$Ba_{(1-y)}O_{(1-x)}Sc_y$
7.3	782.46	560.63	0.99	$Ba_{(1-y)}O_{(1-x)}Al_y$
7.4	783.44	1868.78	1.99	$BaCO_3$
7.5	785.09	1423.08	1.96	$Ba_{(1-y-z)}O_{(1-x)}Sc_yW_z$
7.6	786.38	316.12	1.10	BaO_2

Table 2. Interpretation of electron spectrum of yttrium in the material $90\%BaCO_3 + 10\%Y_2O_3$

№. of peak	Energy of peak, eV	Intensity of peak, counts/s	Width of peak, eV	Yttrium in the phase
1	157.14	24.77	1.95	$3d_{5/2}$ — $Y_{(2-y)}O_{(3-x)}Ba_y$
2	158.74	103.36	1.61	$3d_{3/2}$ — $Y_{(2-y)}O_{(3-x)}Ba_y$
3	159.90	223.86	1.58	$3d_{5/2}$ — $Y_2O_{(3-x)}$
4	161.64	133.73	1.50	$3d_{3/2}$ — $Y_2O_{(3-x)}$

Table 3. Diagram of interpretation of peaks of characteristic losses in the material $90\%BaCO_3 + 10\%Y_2O_3$

№. of peak	ΔE, eV	Width, eV	Series						
			$BaO_{(1-x)}$			$Ba_{(1-y)}O_{(1-x)}Y_y$		$Ba_{(1-y-z)}O_{(1-x)}Ni_yY_z$	
			1	2	3	4	5	6	7
0	0	0	$0E_{S1}$	$0E_{D1}$		$0E_{S2}$	$0E_{D2}$	$0E_{S3}$	$0E_{D3}$
1	2.05	1.08	$1E_{S1}$						
2	3.23	1.96		$1E_{D1}$	$0E_{S1} + 1E_{D1}$				
3	4.17	0.76	$2E_{S1}$						
4	5.03	1.52			$1E_{S1} + 1E_{D1}$				
5	5.61	0.68				$1E_{S2}$			
6	6.52	1.52	$3E_{S1}$	$2E_{D1}$					
7	7.67	1.55			$2E_{S1} + 1E_{D1}$		$1E_{D2}$	$1E_{S3}$	
8	8.46	0.74	$4E_{S1}$						
9	9.27	1.65		$3E_{D1}$	$3E_{S1} + 1E_{D1}$				
10	10.00	0.88	$5E_{S1}$						
11	11.01	1.62			$4E_{S1} + 1E_{D1}$	$2E_{S2}$			$1E_{D3}$
12	12.36	1.22	$6E_{S1}$						
13	13.27	0.78		$4E_{D1}$	$5E_{S1} + 1E_{D1}$				
14	14.39	1.49	$7E_{S1}$						
15	15.65	1.18			$6E_{S1} + 1E_{D1}$		$2E_{D2}$	$2E_{S3}$	
16	16.44	0.84	$8E_{S1}$	$5E_{D1}$					
17	17.41	1.89			$7E_{S1} + 1E_{D1}$	$3E_{S2}$			
18	19.20	1.31	$9E_{S1}$	$6E_{D1}$	$8E_{S1} + 1E_{D1}$				
19	20.93	1.99	$10E_{S1}$						
20	21.78	0.67			$9E_{S1} + 1E_{D1}$				$2E_{D3}$
21	22.84	1.69	$11E_{S1}$	$7E_{D1}$		$4E_{S2}$	$3E_{D2}$	$3E_{S3}$	
22	23.91	0.72			$10E_{S1} + 1E_{D1}$				
23	24.58	1.42	$12E_{S1}$						
24	26.54	0.91	$13E_{S1}$	$8E_{D1}$	$11E_{S1} + 1E_{D1}$				
25	27.86	0.61			$12E_{S1} + 1E_{D1}$	$5E_{S2}$			
26	29.40	0.44	$14E_{S1}$	$9E_{D1}$	$13E_{S1} + 1E_{D1}$				

Table 4. Identification of series of characteristic losses in the material $90\%BaCO_3 + 10\%Y_2O_3$

№. of series	Equation of series	E_S, eV	E_D, eV	$\bar{E}_S$, eV	$\bar{E}_D$, eV
1	$\Delta E = E_{S.1} \cdot n_2$	2.10	–	2.06	3.36
2	$\Delta E = E_{D.1} \cdot n_1$	–	3.27		
3	$\Delta E = E_{S.1} \cdot n_2 + E_{D.1}$	2.01	3.45		
4	$\Delta E = E_{S.2} \cdot n_2$	5.57	–	5.57	7.61
5	$\Delta E = E_{D.2} \cdot n_1$	–	7.61		
6	$\Delta E = E_{S.3} \cdot n_2$	7.61	–	7.61	10.89
7	$\Delta E = E_{D.3} \cdot n_1$	–	10.89		

Note. The indices „S“ and „D“ are related to the surface and volume parameters, accordingly. Two right columns include averaged values.

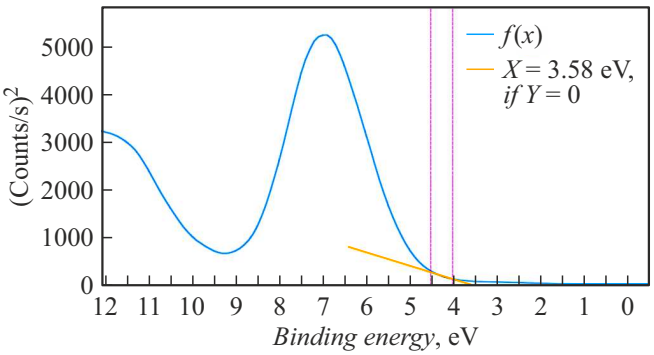

Figure 5. The structure of the edge of the valence band of the sample of material $BaCO_3 + 10\%Y_2O_3$, annealed in the vacuum at 1200°C during 2 h in the coordinates „signal intensity square−bond energy“.

2. Experimental results and discussion thereof

Table 1 includes summary of the results of interpretation of chemical states of barium in the studied samples. Position of barium peaks in phases $Ba(OH)_2 \cdot H_2O$, $BaO_{(1-x)}$, $Ba_{(1-y)}O_{(1-x)}W_y$, $2.5BaO \cdot 0.4CaO \cdot Al_2O_3$, $Ba_{(1-y)}O_{(1-x)}Ca_y$, $BaCO_3$, $Ba_{(1-y)}O_{(1-x)}Al_y$, $Ba_{(1-y)}O_{(1-x)}Sc_y$, BaO_2 is in a good coherence with the data given in [14]. This also allowed interpretation of the peaks of barium states in BaO crystallites alloyed with yttrium, rhenium, palladium, strontium, including, when alloying with two types of atoms. The obtained results confirm the above assumption that in the process of formation of active emission BaO crystallites containing oxygen vacancies in the studied samples of materials, the BaO crystallites are also formed, alloyed with one or two types of micro admixtures of the elements originated from their phase composition.

In Table 2 given as an example it can be seen that in the sample of material $90\%BaCO_3 + 10\%Y_2O_3$, yttrium oxide crystallites containing the oxygen vacancies are also being formed simultaneously in the process of heating in the vacuum, as well as yttrium oxide crystallites that contain oxygen vacancies and micro admixtures of barium atoms. This result is important for understanding of physical and chemical processes flowing in other types of cathode materials — high-temperature cathodes based on the yttrium oxide and tantalum (sintered cathodes) and yttrium oxides, aluminum oxide and tungsten (metal ceramic cathodes), that have become applicable in high-power microwave magnetrons.

As it can be seen from the list of characteristic losses of energy of electrons in the sample of material $90\%BaCO_3 + 10\%Y_2O_3$ (Table 3), all peaks can be grouped into several series, which are described by the equation (2). These series, given as an example for the material $90\%BaCO_3 + 10\%Y_2O_3$ in Table 4, allow to determine the energies of surface and volume plasmons and to calculate the values of volume and surface concentrations of oxygen vacancies for oxide phases and the values of volume and surface electron concentration for metallic phases. Similar results were obtained also for other studied materials. Table 5 includes summary of the data for the parameters of electron structure of phases formed in the composition of the studied samples of materials as a result of their annealing in vacuum. In the interpretation of phases in Table 5 the results of Table 1 were taken into consideration, as well as attention was paid to the value of intensity of peaks of characteristic losses given in Fig. 6 as an example for the material $90\%BaCO_3 + 10\%Y_2O_3$. The phases highlighted bold in the right column of Table 5 refer to those with the minimum values of ratio of the surface and volume concentration of oxygen vacancies.

In order to determine the impact of the phase state of scandium (forming part of oxide, intermetallic compound, hydride) in the cathode material to the process of formation of oxygen vacancies in BaO crystallites, Fig. 6 shows the concentration dependencies (on the content of scandium oxide) of the volume and surface concentrations of oxygen vacancies in the samples of

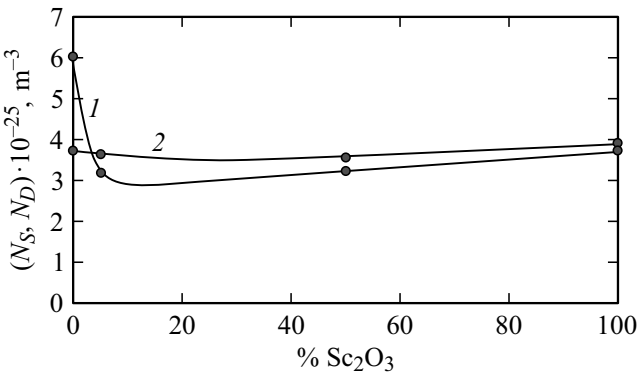

Figure 6. Dependences of the volume (*1*) and surface (*2*) concentrations of oxygen vacancies on the content of Sc_2O_3 in cathode materials.

Table 5. Parameters of characteristic losses (E_S, E_D), as well as concentrations of oxygen vacancies (N_S, N_D) in cathode materials

№. of phase	Phase	Parameter				
		E_S, eV	E_D, eV	N_S, m^{-3}	N_D, m^{-3}	N_S/N_D
1	$90\%BaCO_3 + 10\%Y_2O_3$					
1.1	$Ba_{(1-y)}O_{(1-x)}Y_y$	2.06	3.36	$5.38 \cdot 10^{24}$	$7.15 \cdot 10^{24}$	**0.75**
1.2	$BaO_{(1-x)}$	5.57	7.61	$4.45 \cdot 10^{25}$	$4.15 \cdot 10^{25}$	1.07
1.3	$Ba_{(1-y-z)}O_{(1-x)}Ni_yY_z$	7.61	10.89	$4.53 \cdot 10^{25}$	$4.63 \cdot 10^{25}$	0.98
2	$90\%BaCO_3 + 10\%Re$					
2.1	$BaO_{(1-x)}$	2.23	2.89	$6.30 \cdot 10^{24}$	$5.29 \cdot 10^{24}$	1.19
2.2	$Ba_{(1-y)}O_{(1-x)}Re_y$	3.78	5.03	$1.55 \cdot 10^{25}$	$1.37 \cdot 10^{25}$	1.13
2.3	$Ba_{(1-y-z)}O_{(1-x)}Ni_yRe_z$	7.21	10.05	$4.06 \cdot 10^{25}$	$3.95 \cdot 10^{25}$	**1.03**
3	$90\%BaCO_3 + 10\%Pd$					
3.1	$BaO_{(1-x)}$	2.43	3.08	$7.48 \cdot 10^{24}$	$6.01 \cdot 10^{24}$	1.25
3.2	$Ba_{(1-y)}O_{(1-x)}Pd_y$	3.83	5.49	$1.26 \cdot 10^{25}$	$1.33 \cdot 10^{25}$	0.95
3.3	$Ba_{(1-y-z)}O_{(1-x)}Ni_yPd_z$	7.36	10.62	$4.23 \cdot 10^{25}$	$4.41 \cdot 10^{25}$	**0.96**
4	$90\%BaCO_3 + 10\%SrCO_3$					
4.1	$BaO_{(1-x)}$	2.20	2.90	$6.13 \cdot 10^{24}$	$5.33 \cdot 10^{24}$	1.15
4.2	$Ba_{(1-y-z)}O_{(1-x)}Ni_ySr_z$	3.82	5.79	$1.72 \cdot 10^{25}$	$1.97 \cdot 10^{25}$	**0.87**
4.3	$Ba_{(1-y)}O_{(1-x)}Sr_y$	7.78	11.29	$4.73 \cdot 10^{25}$	$4.98 \cdot 10^{25}$	0.94
5	$90\%W + 5\%2.5BaO \cdot 0.4CaO \cdot Al_2O_3 + 5\%Re_2Sc$					
5.1	$Ba_{(1-y)}O_{(1-x)}Sc_y$	2.22	3.41	$6.25 \cdot 10^{24}$	$7.37 \cdot 10^{24}$	**0.85**
5.2	$Ba_{(1-y)}O_{(1-x)}W_y$	8.61	11.72	$1.32 \cdot 10^{26}$	$1.22 \cdot 10^{26}$	1.08
5.3	$Ba_{(1-y-z)}O_{(1-x)}Re_ySc_z$	8.80	12.24	$8.41 \cdot 10^{25}$	$8.14 \cdot 10^{25}$	1.03
5.4	W	7.82	11.26	$8.89 \cdot 10^{28}$	$9.21 \cdot 10^{28}$	0.97
6	$90\%W + 5\%2.5BaO \cdot 0.4CaO \cdot Al_2O_3 + 5\%(80\%W + 20\%Re)$					
6.1	$BaO_{(1-x)}$	2.35	3.23	$7.00 \cdot 10^{24}$	$6.61 \cdot 10^{24}$	1.06
6.2	$Ba_{(1-y-z)}O_{(1-x)}Re_yW_z$	5.81	8.85	$3.67 \cdot 10^{25}$	$4.26 \cdot 10^{25}$	**0.86**
6.3	$Ba_{(1-y)}O_{(1-x)}Re_y$	9.70	13.50	$1.68 \cdot 10^{26}$	$1.63 \cdot 10^{26}$	1.03
6.4	W	7.86	10.94	$8.98 \cdot 10^{28}$	$8.70 \cdot 10^{28}$	0.72
7	$90\%W + 5\%2.5BaO \cdot 0.4CaO \cdot Al_2O_3 + 5\%ScH_2$					
7.1	$Ba_{(1-y)}O_{(1-x)}Sc_y$	2.15	3.58	$5.86 \cdot 10^{24}$	$8.12 \cdot 10^{24}$	**0.72**
7.2	$Ba_{(1-y-z)}O_{(1-x)}Sc_yW_z$	5.40	8.09	$1.86 \cdot 10^{25}$	$2.09 \cdot 10^{25}$	**0.89**
7.3	W	7.27	10.23	$7.68 \cdot 10^{28}$	$7.60 \cdot 10^{28}$	1.01

Note. The indices „*S*“ and „*D*“ are related to the surface and volume parameters, accordingly.

materials based on the powders of tungsten and the phase $2.5BaO \cdot 0.4CaO \cdot Al_2O_3$, in which aluminum oxide is fully or partially replaced with the scandium oxide [14]. According to Fig. 6, in wide interval of the scandium oxide content the ratio of surface and volume concentration of vacancies remains the same and equal to 1.1, which is in contrast to the highlighted cells in the right column of Table 5.

When studying the position of the top edge of the valence band in oxide phases by ESCA method, as shown in Fig. 5, there is no possibility of separate determination of the position of edge of the valence band for each oxide phase

Table 6. Parameters of curvature of energetic bands near to the surface of barium oxide crystallites (V)

Parameter	Sample of material					
	$BaCO_3$ [9]	$BaCO_3 + CaCO_3$ [9]	$BaCO_3 + Y_2O_3$	$BaCO_3 + Re$	$BaCO_3 + Pd$	$BaCO_3 + SrCO_3$
E_{VS}, eV	2.70	2.75	**4.15**	3.45	**3.83**	3.48
V, eV	1.33	1.28	**−0.12**	0.58	**0.20**	0.55

individually in case, when there are several oxide phases. At the same time, the total position of the top of the valence band determines the value of total curvature of the energetic bands, i.e. the value of the material work function. Table 6 includes the values of position of the top of the valence band relative to the Fermi level (E_{VS}) and the value of total curvature of energetic bands (V) of barium oxide crystallites for the studied materials. Optimum variants of BaO micro alloying are highlighted bold.

When annealing the barium carbonate or barium-calcium aluminate in vacuum in presence of other phases, the steady-state volume concentration of oxygen vacancies in BaO crystallites depends not only on the original phase composition of the material, but also on the annealing temperature and time, material porosity and grain-size composition of powder components. Merely, it is the optimization of grain-size composition, porosity, annealing temperature and time, which make the activation of cathode material, as a result of which, the necessary concentration of oxygen vacancies is formed in the volume of BaO crystallites. However, the top monolayer of BaO crystallites at any moment of time is thermodynamically balanced with the volume of BaO, at that

— the surface concentration of vacancies, as shown for the first time in [13] and can be seen from the results hereof, is determined not only by the balance between the volume and surface of crystallite, but the presence of alloying (admixture) atoms in the top monolayer of crystallite as well;

— in turn, it is the surface concentration of oxygen vacancies determines the value of curvature of energetic bands near to the surface of barium oxide crystallites: the less the value of curvature, the less the value of work function [13].

The study [13] proposed a theory of scandate cathodes, according to which a low work function of the barium oxide crystallite can be ensured by forming the BaO nanocrystallite, in the top monolayer of which barium atoms are fully or partially replaced with the scandium atoms. An indication of formation of such structure is decrease of the surface concentration of oxygen vacancies compared to the volume concentration of oxygen vacancies. The pre-condition for formation of such structure is dimensional factor of alloying element; its ion radius must be equal to about 0.60 of the barium ion radius. This criterion also covers nickel, whose ion radius is 0.54 of that of barium. Based on the theoretical approach [13] one can define more general conditions that ensure decrease of the surface concentration of oxygen vacancies in barium oxide crystallites relative to its volume concentration and being generalization of the study [13] and experimental results hereof:

— the enthalpy of formation of the alloying element oxide must be higher than the enthalpy of the barium oxide formation, i.e. the bond energy of „oxygen ion−alloying element ion“ must be higher than the bond energy of „oxygen ion−barium ion“;

— for efficient alloying of barium oxide crystallites with other element, the latter in original phase must be in a weakly bound form, e.g., as a part of intermetallic compound, hydride or nanocrystallic oxide with a high excessive surface energy;

— for segregation of the alloying element, it is the top monolayer of barium oxide crystallite, where the crystallite in question must be in the form of nanocrystals, with a high difference of the inter-plane distance between the first and the second monolayers and monolayers in the volume of nanocrystallite. It is the case, when the dimensional factor of the alloying element starts playing the role.

These conditions, as it can be seen in Table 5, are met when adding additional components in the form of intermetallic compound Re_2Sc and hydride ScH_2 into original barium carbonate, which are met at a low content of additional component in the form of the scandium oxide and violated at a high concentration of the scandium oxide in the material. The same conditions are met also in case of joint alloying of barium oxide with nickel and strontium, it is what high thermal emission properties of oxide-nickel cathodes are based on.

Conclusion

1. Criteria of achievement of the minimum work function of the cathode material with BaO crystallites as an active emission component refer to the provision of the minimum ratio of surface and volume concentration of oxygen vacancies in BaO and the maximum distance between the top of the valence band and the Fermi level with BaO.

2. High thermal emission properties of scandate cathode could be ensured by formation in the cathode material of barium oxide crystallites, in the top monolayer of which barium atoms are fully or partially replaced with scandium atoms.

3. Efficient alloying of crystallites with scandium atoms can be ensured when using scandium in the composition of the cathode material; scandium in the composition of the scandium intermetallic compound, scandium hydride or scandium oxide in the nanocrystal state.

4. Ensuring segregation of scandium atoms in the top monolayer of barium oxide crystallites is possible through formation of these crystallites at the stage of cathode activation in the form of nanocrystallites of barium oxide.

5. Formation of the nanocrystallites of barium oxides at the stage of the cathode activation is possible by using the barium-calcium aluminate (tungsten) decomposition activator in the form of tungsten nanocrystals or vapors of low tungsten oxides transported to the aluminate surface from the volume of cathode through the pores in aluminate.

Conflict of interest

The authors declare that they have no conflict of interest.

References

[1] G. Gartner, P. Geintter, A. Ritz. Appl. Surf. Sci., **111**, 11 (1997).
[2] I.I. Bekh, O.I. Getman, V.V. Il'chenko, A.E. Lushkin, V.V. Panichkina, S.P. Rakitin. Ukr. J. Phys., **54** (3), 297 (2009).
[3] I. Brodie, B. Vancil. Proc. IEEE Int. Vacuum Electron. Conf., Monterey, CA, United States. 2014. P. 53–54.
[4] C. Lai, J.S. Wang, F. Zhou, W. Liu, P. Hu, C.H. Wang, R.Z. Wang, N.H. Miao. Appl. Surf. Sci., **440**, 763 (2018).
[5] X. Liu, B. Vancil, M. Beck, T. Balk. Materials, **12**, 636 (2019).
[6] F. Yang, J. Wang, W. Liu, Y. Wang, M. Zhou. Proc. IEEE Int. Vacuum Electron. Conf., Monterey, CA, United States. 2014. P. 55–56.
[7] V.I. Kapustin. Izvestiya AN SSSR, ser. fiz., **55** (12), 2455 (1991) (in Russian).
[8] V.I. Kapustin. Perspektivnye materialy, **2**, 5 (2000) (in Russian).
[9] V.I. Kapustin, I.P. Li, V.S. Petrov, N.E. Ledentsova, A.V. Turbina. Elektronnaya tekhnika, ser. 1: SVCh-tekhnika, **1** (528), 8 (2016) (in Russian).
[10] I.P. Li, V.S. Petrov, T.V. Prokofieva, N.E. Ledentsova, A.V. Shumanov, A.D. Silaev, V.S. Polyakov, V.I. Kapustin, V.I. Svitov. Elektronnaya tekhnika, ser. 1: SVCh-tekhnika, **2** (525), 45 (2015) (in Russian).
[11] V.I. Kapustin, I.P. Li, A.V. Shumanov, Yu.Yu. Lebedinskii, A.V. Zablotskii. Tech. Phys., **62** (1), 116 (2017).
[12] V.I. Kapustin, I.P. Li, A.V. Shumanov, S.O. Moskalenko, V.I. Svitov. Inorganic Mater.: Appl. Res., **10** (5), 1065 (2019).
[13] V.I. Kapustin, I.P. Li, A.V. Shumanov, S.O. Moskalenko. Tech. Phys., **65** (1), 151 (2020).
[14] V.I. Kapustin, I.P. Li. *Teoriya, elektronnaya struktura i fizikokhimiya materialov katodov SVCh priborov* (INFRA-M, M., 2020) (in Russian).